Research Article Vol. 29, No. 2 / 18 January 2021 / Optics Express 929
Optics EXPRESS

Ultrashort visible energetic pulses generated by nonlinear propagation of necklace beams in capillaries

AURORA CREGO,* ENRIQUE CONEJERO JARQUE, AND JULIO SAN ROMAN

Grupo de Investigación en Aplicaciones del Láser y Fotónica, Departamento de Física Aplicada, University of Salamanca, Salamanca E- 37008, Spain
acrego@usal.es

Abstract: The generation of ultrashort visible energetic pulses is investigated numerically by the nonlinear propagation of infrared necklace beams in capillaries. We have developed a (3+1)D model that solves the nonlinear propagation equation, including the complete spatio-temporal dynamics and the azimuthal dependence of these structured beams. Due to their singular nonlinear propagation, the spectrum broadening inside the capillary extends to the visible region in a controlled way, despite the high nonlinearity, avoiding self-focusing. The results indicate that the features of these necklace beams enable the formation of visible pulses with pulse duration below 10 fs and energies of 50 μJ by soliton self-compression dynamics for different gas pressures inside the capillary.

1. Introduction

In the last decades, several schemes have been developed to obtain ultrashort pulses in different bands of the visible spectral region as an important tool for different applications, such as ultrafast spectroscopy or transient absorption image techniques in biomedical science [1,2]. There is a variety of strategies to obtain these sources. If the duration of the pulse is not a crucial factor, praseodymium ion-based mode-locked lasers are a straightforward option to obtain picosecond pulses with high average energy in red and green bands [3,4]. However, if few-cycle pulses are needed, two- or several-step setups have to be used such as cascaded four-wave mixing [5–9], nonlinear optical parametric amplification [1,10], optical parametric chirped pulse amplification with second harmonic generation (SHG) and excimer gas amplification [11], up-conversion of different parts of the spectrum coming from fiber-based ultrafast systems [2], spectral broadening in capillaries [12–15], which are the simplest hollow core fibers (HCFs), or in filaments [16], blueshifting solitons in single-ring photonic crystal fibers [17], or tunable dispersive waves (DWs) generated during the solitonic propagation, also in capillaries [18–20].

Although the techniques described above can deliver ultrashort and energetic pulses in the visible region of the spectrum, the complexity of most of the setups has motivated the search of alternatives. One of the most compact setups to achieve tunable ultrashort pulses, of all those mentioned above, is the DW emission from a solitonic propagation of an infrared laser pulse in capillaries filled with gas [18,20], although the amount of energy transferred to the DW is still limited. One possible solution would be to increase the input pulse energy, but this is also limited by self-focusing and the ionization of the gas inside the capillary [21,22]. Another possibility would be to study the nonlinear propagation of structured laser beams, which can be now easily generated and controlled [23], in a standard post-compression setup so the spectrum could be broadened in a controlled and efficient way to the visible region, yielding ultrashort and energetic pulses.

#411338 https://doi.org/10.1364/OE.411338
Journal © 2021 Received 1 Oct 2020; revised 22 Nov 2020; accepted 26 Nov 2020; published 5 Jan 2021

Optics EXPRESS

In this work we have studied the nonlinear propagation of infrared structured beams, in particular necklace beams (NBs) [24], along a capillary filled with argon. Necklace beams are a type of structured laser beams with amplitude and phase rotational symmetry around the propagation axis. Although they are intrinsically unstable in free propagation, under some circumstances they show self-trapping features which allow them to propagate with minor variations along noticeable distances in different nonlinear media such as Kerr-type media [25], thermal nonlocal media [26], colloidal engineered media [27,28], photorefractive media [29], nonlinear lattice structures [30], or cubic-quintic nonlinear media [31]. By contrast to free propagation, NBs can be stable when propagating inside confined structures [32]. In this work we exploit the features of the nonlinear propagation of NBs inside capillaries to generate ultrashort pulses in the visible region.

There are different families of NBs in a capillary depending on the number of rings and beads they present. According to Marcatili's model [33], a linearly polarized NB can be represented as a composition of two hybrid modes, $EH_{(-|n|)m} + EH_{(|n|+2)m}$, both with the same complex propagation coefficient. Its spatial amplitude can be represented by a radially dependent Bessel function of the first kind with a sinusoidal azimuthal dependence: $J_{n+1}(u_{(n+1)m}r/a)sin\,((n+1)\theta)$, where a is the core size and u_{nm} represent the m-th root of the J_n Bessel function. Although the spatial structure of these modes seems complex, their generation has already been demonstrated [25].

One of the main advantages of these NBs, that makes them an interesting alternative to hybrid modes, is that, since they are composed of higher spatial modes, they present anomalous dispersion for standard capillary core sizes, with gas pressures close to atmospheric pressure in the wavelength region of 0.8 μm, which are standard conditions in the post-compression context. This feature enables the formation of a short pulse at the end of the capillary by soliton self-compression dynamics, as shown in [34,35], so there is no need of an additional compression stage as in [12]. Moreover, the amount of linear dispersion can be easily tuned by changing the gas type or pressure, the capillary core size or the pump wavelength, as usually done in standard post-compression setups.

In this work, we will try to gain some insight into the nonlinear propagation dynamics of a NB inside a gas-filled capillary, using a (3+1)D numerical model based on the nonlinear Schrödinger equation (NLSE).

2. Results and discussion

2.1. Numerical model

To study the nonlinear propagation dynamics of necklace laser beams in capillaries we have developed a (3+1)D numerical model that includes the complete spatio-temporal dynamics. The propagation equation for the envelope of the pulse in cylindrical coordinates, $E(r,\theta,z,t)$, is:

$$\frac{\partial E(r,\theta,z,t)}{\partial z} = (\hat{L}+\hat{N})E(r,\theta,z,t), \tag{1}$$

where the first term, $\hat{L}$, represents the linear effects, namely the diffraction, the linear losses and the dispersion of the laser beam in the capillary. The expressions that we have used for these effects are:

$$\hat{L} = \frac{i}{2k_0}\left(\frac{\partial^2}{\partial r^2}+\frac{1}{r}\frac{\partial}{\partial r}+\frac{1}{r^2}\frac{\partial^2}{\partial\theta^2}\right)-\frac{\alpha}{2}+\sum_{n=2}^{\infty}\frac{i^{n+1}}{n!}\beta_n\frac{\partial^n}{\partial t^n}, \tag{2}$$

where $k_0 = \omega_0/c$, ω_0 being the central frequency and c the speed of light in vacuum, $\beta_n = (\partial^n\beta/\partial\omega^n)_{\omega_0}$, and α and β are the absorption and dispersion coefficient of the input necklace beam obtained from [33], respectively. The second term, $\hat{N}$, represents the most significant nonlinear effects, such as self-phase modulation (and self-focusing), self-steepening, ionization,

Optics EXPRESS

and the losses due to the ionization process and plasma absorption. The expression that we have used for these effects is:

$$\hat{N} = ik_0 n_2 T\left[|E|^2 E\right] - \frac{\sigma}{2}\left(1 + i\omega_0\tau_C\right)T^{-1}\left[\rho E\right] - \frac{W(|E|^2)U_i}{2|E|^2}\left(\rho_{at} - \rho\right)E, \tag{3}$$

where n_2, σ, τ_C, $W(|E|^2)$, U_i and ρ_{at} are different parameters of the gas inside the capillary: the nonlinear refraction index, the cross section for inverse Bremsstrahlung, the collision time, the ionization rate, the ionization potential and the atomic density, respectively. $T = 1 + i/\omega_0(\partial/\partial t)$ is a temporal operator (which is responsible of the self-steepening in the first term of $\hat{N}$) and ρ is the photoionized plasma density inside the capillary, whose evolution is obtained by solving the rate equation $\partial\rho/\partial t = W(|E|^2)(\rho_{at} - \rho)$. The ionization rates are calculated using the PPT model [36]. This model is a 3D extension of the model presented in [37] enhanced to study the nonlinear propagation of beams without cylindrical symmetry through gas-filled capillaries.

We solved Eq. (1) by using a Split-Step Method [38]. The linear part with the azimuthal dependence and the dispersion is solved in the Fourier space, while the linear part with the radial dependence is solved using a Crank-Nicolson algorithm. All the terms of the nonlinear part are solved with a fourth-order Runge-Kutta algorithm in the time domain.

Although we have simulated the nonlinear propagation of different NBs with four, six and eight beads in a Ar-filled capillary, we will discuss mainly the case of the six-bead necklace beam. This spatial mode is a composition of two hybrid modes: EH_{-21} and EH_{41}. We have chosen this spatial mode in particular because it has an anomalous response high enough to self-compress in a standard one meter long capillary without requiring high computational time. The complete expression of the component of the electric field in the core of the capillary is:

$$E(r, \theta, t, z = 0) = J_3\left(u_{31}r/a\right) \cdot sin(3\theta)e^{-t^2/t_0^2}, \tag{4}$$

where u_{31} is the first zero of the Bessel J_3 function, a is the capillary core radius and t_0 is the temporal pulse duration. We propagate a 30-fs pulse with 0.2 mJ input energy at 0.8 μm through a one meter long capillary with 150 μm core radius filled with argon at 1 bar. The gas parameters used in the model for all the cases are presented in Table 1.

Table 1. Parameters for argon, the gas used in the simulations [21]

n_2=1.74 $\cdot$ $10^{23} m^2/W$	σ=$k_0\omega_0\tau_C/(n_0\rho_C(1+\omega_0^2\tau_C^2))$	τ_C=350fs
ρ_C=3.14208 $\cdot$ $10^{20}\omega_0^2 cm^{-3}$	ρ_{at}=2.7 $\cdot$ $10^{19} p(bar) cm^{-3}$	U_i=15.76eV

2.2. Propagation of necklace beams in capillaries

Figure 1 presents the propagation dynamics of the NB inside the capillary, showing the evolution of the spectral distribution in logarithmic scale (left), the temporal distribution in linear scale (center) and the temporal FWHM duration (right) at the point of maximum intensity of one bead. If we look at the spectrum, Fig. 1(left), the pulse begins the propagation in the anomalous dispersion region. Note that for the parameters used in the simulation, the zero dispersion wavelength (ZDW), shown as a black dashed line in the left panel, is 0.68 μm. The nonlinearity is so high in this case, that the spectrum broadens in such a way that concentrates the energy in two spectral bands, as expected in a high soliton order propagation situation (in our case N=14) [38]. While the red-shifted band continues in the anomalous dispersion region, enabling a soliton formation, the other band shifts to the visible part of the spectrum, entering into the normal dispersion regime. It is important to remark that, although the nonlinearity is high, we have not observed any spatial dynamics related to self-focusing, so the beam keeps the same six-bead intensity structure during the whole propagation (see the movies included in Fig. 1 as

Optics EXPRESS

Suppl. Material). Moreover, we have checked that the effect of the ionization in the propagation dynamics is also negligible.

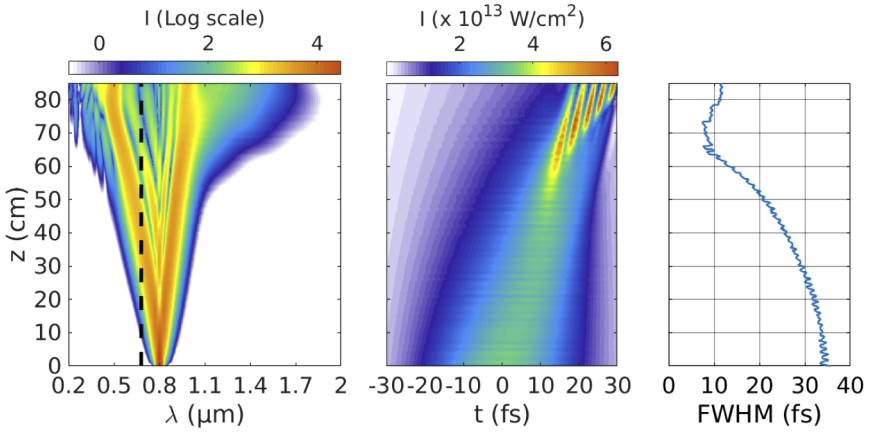

Fig. 1. The figure shows the evolution of the spectral intensity distribution in log scale (left), of the temporal intensity distribution in linear scale (center) and of the temporal FWHM (right), evaluated at the peak intensity of one bead of the NB. The black dashed line in the left panel corresponds to the zero dispersion wavelength (0.68 μm). The beam keeps its spatial structure during the whole propagation (Visualization 1 shows the complete spatio-temporal evolution of the beam). A similar propagation is obtained for a four-bead NB (see Visualization 2) and an eight-bead NB (see Visualization 3).

The spectral dynamics is accompanied by a self-compression process and the generation of a solitonic structure around 66 cm inside the capillary, as can be seen in Fig. 1(center). During the self-compression process the peak of the intensity distribution is delayed (shifted towards positive time values) and, at the same time, the pulse is becoming slightly distorted, with the peak shifted towards the rear part of the pulse. Both effects are induced by the self-steepening effect, which plays an important role in this self-compression process. The strong shock formation typically related to self-steepening is, in this case, dissipated by the dispersion. As a consequence of the temporal delay of the whole pulse, the high-order soliton appears also at a delayed time.

The evolution of the pulse duration at its full width half maximum (FWHM) is shown in Fig. 1(right). We can see that the pulse reaches a minimum pulse duration of 7.5 fs at 66 cm inside the capillary, where the solitonic structure appears. From that point, the higher order dispersion terms cause the pulse fission, where the pulse breaks up in subpulses and there is no further spectral broadening.

The two-band structure of the spectrum suggests the possibility of filtering the visible band to see if we are able to obtain an ultrashort visible energetic pulse. For this purpose, we have filtered the visible band using a square dynamic filter that takes the main part of the band at each point. In Fig. 2(left) we show the filtered spectrum (in logarithmic scale) from the point at which the band is in the normal dispersion region, around 45 cm inside the capillary. As we can see, after the band crosses the ZDW it continues shifting to shorter wavelengths along the propagation, without changing its width or structure, until it reaches a wavelength of 0.55 μm, where the soliton fission occurs. From the temporal point of view, see Fig. 2(center), the peak intensity of the visible band is always of the order of 4×10^{13} W/cm^2, with a similar temporal structure with few femtoseconds of duration. Figure 2(right) shows the evolution of the energy (blue line), the temporal FWHM duration (solid orange line) and the temporal FWHM duration of the Fourier Limit (orange dashed line) of the filtered band. The energy of the band grows during the propagation until the band crosses the ZDW, when it reaches around 50 μJ. From

Optics EXPRESS

that point on, the energy remains quite constant without presenting relevant losses during the propagation until the soliton fission occurs. Regarding the temporal duration of the visible band, we can see that the FWHM is always less than 10 fs and very close to its Fourier Limit, which indicates that the phase structure of the visible band is very flat.

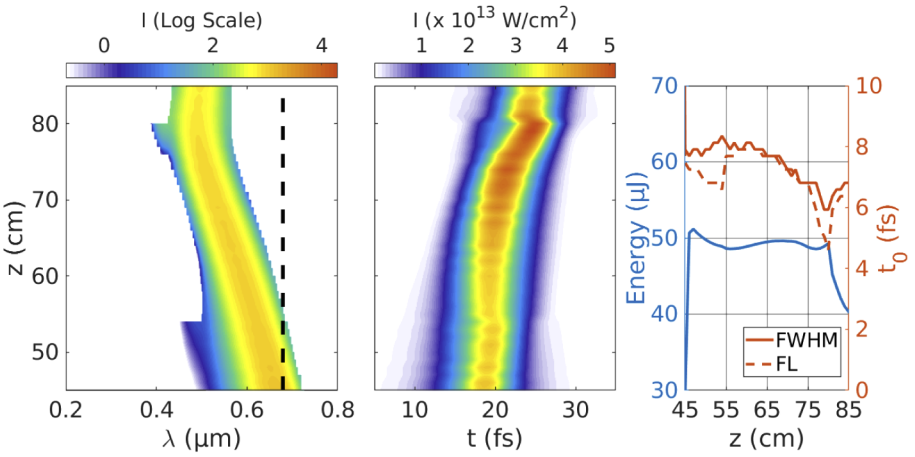

Fig. 2. The figure shows the evolution of the spectral intensity distribution in log scale (left), of the temporal intensity distribution in linear scale (center) and the energy (blue line), the temporal FWHM (orange line) and Fourier limit (orange dashed line) of the visible band, evaluated at the peak intensity of one bead of the NB. The black dashed line in the left panel corresponds to the zero dispersion wavelength (0.68 μm).

Now that we have demonstrated that we are able to generate ultrashort visible energetic pulses, it would be interesting to understand its dependence with different parameters of the capillary. The easiest one to change in a real experiment is the pressure inside the capillary. For this reason we have performed the same study as before, but for different constant pressures inside the capillary. We compare the visible bands of the spectrum, generated in each case, at the same distance where the self-compression was optimum for the 1 bar case, at 66 cm, as if it were the actual capillary length. In Fig. 3(left) we compare the visible band obtained for different pressures inside the capillary, scanned from 0.5 to 1.2 bar. We have observed that the band suffers a blue-shift as the pressure inside the capillary increases, which comes from the higher nonlinearity and the induced spectral broadening. This spectral shift saturates when the band reaches the 0.55 μm region due to the appearance of the soliton fission dynamics, that stops the spectral shift of that band. It is not surprising that the role of the pressure in the spectral tunability of this visible pulse is the opposite to the case of DW signals, for which increasing the pressure provides longer wavelengths [18,20], since their nonlinear origins are different.

We have also calculated the energy and the temporal duration of the bands at 66 cm inside the capillary to observe the dependence with the pressure. The blue triangles in Fig. 3(right) show that the energy of the visible band is quite constant, being always around 50 μJ, which is a significant amount of energy. The amount of energy in the visible band of the spectrum goes from 23% to 27% of the total input pulse energy and from 34% to 40% of the total pulse energy at 66 cm. The orange circles in Fig. 3(right) correspond to the temporal duration at FWHM of the pulse obtained from the visible band (solid line) and its Fourier Limit (dashed line). As we can see, the pulse duration is always below 10 fs, reaching 5 fs of duration at the cases with 0.6-0.8 bar of pressure. Unfortunately, in this optimum region the spectral phase of the output pulse is not perfectly balanced, and it could be post-compressed to a Fourier Limit pulse of 3 fs

Optics EXPRESS

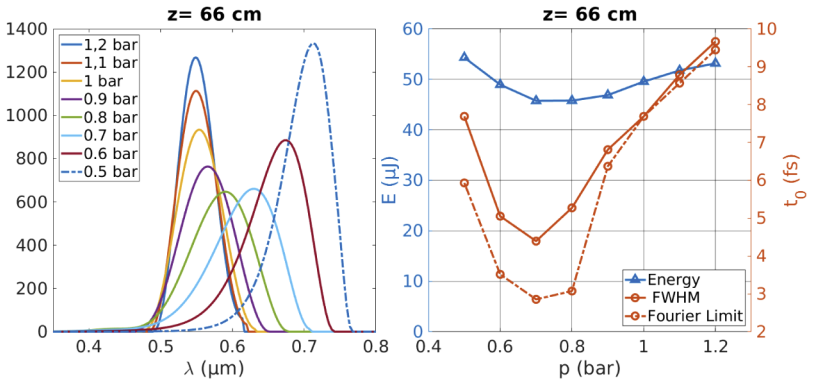

Fig. 3. This figure shows the comparison of the spectral bands in the normal dispersion region (left) and the comparison of the energies and pulse duration of each band (right), both for different constant pressures inside the capillary at 66 cm.

of duration. Nevertheless, all the pulses obtained are good ultrashort visible energetic pulses, according to the literature.

2.3. *Spatial robustness of the beam along the capillary*

In this subsection we would like to see what occurs if the input beam profile is not ideal. First of all, we should emphasize that we wanted to avoid any self-focusing effect, so the energy regime that we have used was chosen so the spectral broadening was enough to reach the visible part of the spectrum, that was our main objective, but without entering in the self-focusing regime. For this reason, we forced us to be below the critical power of a Gaussian beam, $P = 0.96P_{cr}$, so even one bead carrying all the energy would not be able to collapse [25]. Under these conditions we have demonstrated that a pure necklace beam shows a nice spectral broadening, keeping a very good spatial quality and without any spatial collapse.

According to the literature, in the situation of a non-ideal six-bead input beam, it would become unstable during the nonlinear propagation inside the capillary if the input power is above $0.36P_{cr}$ [32]. As we are well above this threshold, we should see an energy transfer between beads that becomes more significant as the beam propagates inside the capillary. To test numerically how relevant this situation could be, we have simulated the propagation of the same six-bead necklace beam presented in Fig. 1, but with one of the beads (labelled “B #1" in the figures below) having 5% more energy, as is usually done in similar stability analyses [32]. As expected, there is an energy transfer between beads but, in the moderate power regime that we use, the six-bead structure holds during the whole propagation distance. Figure 4(left) shows the beam fluence, i.e. the temporal integration of the spatio-temporal intensity for the non-ideal case, at the self-compression position of the pure input case (z=66 cm). As it can be observed, the 6 bead-structure is kept and, although during the propagation some of the beads acquire high peak intensity values, we have not observed any self-focusing dynamics.

Figure 4(middle and right) represents the spectral and temporal distribution of beads #1 and #4 at z=66 cm, together with the weighted average spectral or temporal distribution from the non-ideal beam and the comparison with the ideal beam presented in the previous subsection. This weighted average is calculated taking into account the relative energy of each bead. It is clear that the spectral broadening towards the visible and the temporal self-compression are still there but, of course, not equally in all the beads of the beam. These observations are easily explained because not all beads carry the same amount of energy during the propagation. We see that there are only some beads of the beam that reach high peak intensity values during the propagation,

Optics EXPRESS

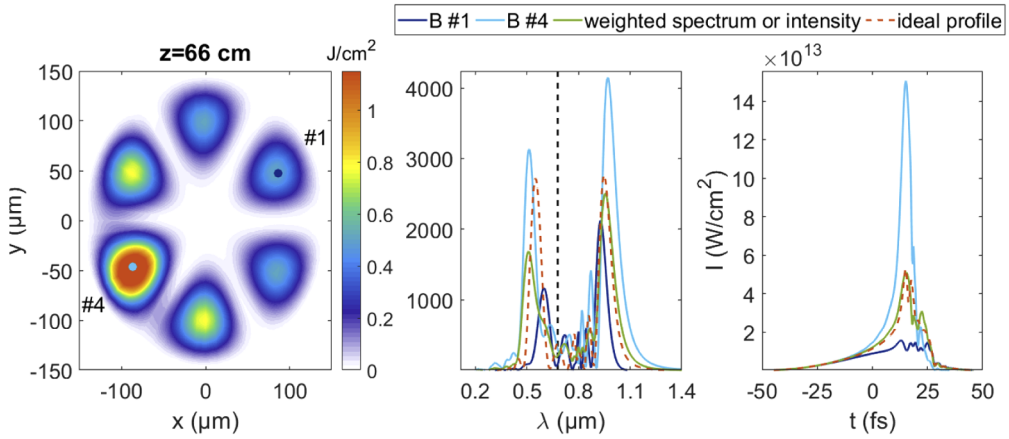

Fig. 4. The left panel shows the beam fluence of a non-ideal six-bead input beam at z=66 cm. The simulation parameters used here are the same as those used in Fig. 1, although starting with a perturbed spatial beam. The middle and right panel show the spectrum and temporal distribution, respectively, of the peak intensity points of two different beads and the weighted average spectral and temporal intensity distribution at z=66 cm. We can see that the spectrum and temporal structure is similar to the ideal case (orange dashed lines).The black dashed line shows the ZDW. Visualization 4 shows the complete spatio-temporal evolution of the non-ideal beam.

in our case only beads #1 and #4, and only those are able to self-compress as the ideal beam. Moreover, these beads are located opposite to each other, so they do not self-compress at the same propagation distance. We have calculated the weighted average spectral and temporal distribution in the non-ideal case at 66 cm and we have compared it with the ideal case, we can observe that they are quite similar (see Fig. 4 (middle and right)). In view of the spatial profile at 66 cm shown in Fig. 4(left), we can identify the optimal bead and select it. The spatial selection of part of the beam would produce a decrease of the output energy to 14.6 μJ for bead #4 at z=66 cm. If we filter the visible band, considering the weighted average spectral distribution at 66 cm, and calculate the energy in the non-ideal case for the whole beam, we then obtain 37.3 μJ, which is not far from the ideal case. On the other hand, Fig. 4(right) indicates that the self-compression of the selected bead could be even better compared to the ideal case, going from a temporal FWHM of 7.5 fs in the ideal case to a FWHM of 6.15 fs in bead #4 in the non-ideal case. Therefore, it is true that this non-ideal situation would somehow deteriorate the output pulse, basically the output energy, but it will still be useful. Moreover, we must emphasize that we are in a power regime in which the instability is not large enough to couple all the energy into one bead and activate a self-focusing process.

3. Conclusion

In conclusion, high-energy ultrashort pulses in the visible region of the spectrum can be generated in standard capillaries with infrared necklace beams as driving pulses. We have found that the high nonlinearity broadens the spectrum in such a way that the energy is concentrated in two bands, one of them reaching the visible part of the spectrum during the propagation. Filtering this spectral band, we can obtain pulse energies of around 50 μJ and pulse durations below 10 fs using a 150 μm core radius capillary filled with argon. The high efficiency (25%) and the wavelength tunability for different gas pressures inside the capillary, demonstrate that the soliton self-compression of infrared necklace beams in capillaries filled with gas could be a compact tool which paves the way to new short laser pulse sources in the visible region. We have

Optics EXPRESS

also demonstrated that when using non-ideal input necklace beams, where there is a nonlinear energy transfer between the beads, they still present a similar spectral band and a temporal self-compression, although only in those beads that reach high peak intensity values during the propagation. Even in this non-ideal case, self-focusing does not play a role in the dynamics of the beam.

Funding

Junta de Castilla y León (SA287P18); Ministerio de Economía y Competitividad (BES-2017-080280, FIS2016-75652-P); Ministerio de Ciencia e Innovación (PID2019-106910GB-I00).

Disclosures

The authors declare no conflicts of interest.

References

1. T. Kobayashi, A. Yabushita, and Y. Kida, "Development of sub 10 fs visible-NIR, UV, and DUV pulses and their applications to ultrafast spectroscopy," Photonics **3**(4), 64 (2016).
2. S. R. Domingue, R. A. Bartels, A. J. Chicco, and J. W. Wilson, "Transient absorption imaging of hemes with 2-color, independently tunable visible-wavelength ultrafast source," Biomed. Opt. Express **8**(6), 2807–2821 (2017).
3. S. Luo, B. Xu, H. Xu, and Z. Cai, "High-power self-mode-locked Pr:YLF visible lasers," Appl. Opt. **56**(34), 9552–9555 (2017).
4. N. Li, J. Huang, B. Xu, Y. Cai, J. Lu, L. Zhan, Z. Luo, H. Xu, Z. Cai, and W. Cai, "Direct generation of an ultrafast vortex beam in a CVD-graphene-based passively mode-locked Pr:$LiYF_4$ visible laser," Photonics Res. **7**(11), 1209–1213 (2019).
5. J. Liu and T. Kobayashi, "Generation of sub-20-fs multicolor laser pulses using cascaded four-wave mixing with chirped incident pulses," Opt. Lett. **34**(16), 2402–2404 (2009).
6. J. Liu and T. Kobayashi, "Generation of μJ multicolor femtosecond laser pulses using cascaded four-wave mixing," Opt. Express **17**(7), 4984–4990 (2009).
7. J. L. Silva, R. Weigand, and H. M. Crespo, "Octave-spanning spectra and pulse synthesis by nondegenerate cascaded four-wave mixing," Opt. Lett. **34**(16), 2489–2491 (2009).
8. R. Weigand, J. T. Mendonça, and H. M. Crespo, "Cascaded nondegenerate four-wave-mixing technique for high-power single-cycle pulse synthesis in the visible and ultraviolet ranges," Phys. Rev. A **79**(6), 063838 (2009).
9. J. He, J. Liu, and T. Kobayashi, "Tunable multicolored femtosecond pulse generation using cascaded four-wave mixing in bulk materials," Appl. Sci. **4**(3), 444–467 (2014).
10. K. Okamura and T. Kobayashi, "Octave-spanning carrier-envelope phase stabilized visible pulse with sub-3-fs pulse duration," Opt. Lett. **36**(2), 226–228 (2011).
11. R. Clady, G. Coustillier, M. Gastaud, M. Sentis, P. Spiga, V. Tcheremiskine, O. Uteza, L. D. Mikheev, V. Mislavskii, J. P. Chambaret, and G. Cheriaux, "Architecture of a blue high contrast multiterawatt ultrashort laser," Appl. Phys. B **82**(3), 347–358 (2006).
12. M. Nisoli, S. De Silvestri, and O. Svelto, "Generation of high energy 10 fs pulses by a new pulse compression technique," Appl. Phys. Lett. **68**(20), 2793–2795 (1996).
13. F. Silva, B. Alonso, W. Holgado, R. Romero, J. S. Román, E. C. Jarque, H. Koop, V. Pervak, H. Crespo, and I. J. Sola, "Strategies for achieving intense single-cycle pulses with in-line post-compression setups," Opt. Lett. **43**(2), 337–340 (2018).
14. T. Nagy, M. Kretschmar, M. J. J. Vrakking, and A. Rouzée, "Generation of above-terawatt 1.5-cycle visible pulses at 1 kHz by post-compression in a hollow fiber," Opt. Lett. **45**(12), 3313–3316 (2020).
15. S. Palato, H. Seiler, H. Baker, C. Sonnichsen, R. Zifkin, J. McGowan, and P. Kambhampati, "An analysis of hollow-core fiber for applications in coherent femtosecond spectroscopies," J. Appl. Phys. **128**(10), 103107 (2020).
16. B. Spokoyny, C. J. Koh, and E. Harel, "Stable and high-power few cycle supercontinuum for 2D ultrabroadband electronic spectroscopy," Opt. Lett. **40**(6), 1014–1017 (2015).
17. Z. Huang, Y. Chen, F. Yu, D. Wu, D. Wang, R. Zhao, Y. Zhao, S. Gao, Y. Wang, P. Wang, and Y. Leng, "Highly-tunable, visible ultrashort pulses generation by soliton-plasma interactions in gas-filled single-ring photonic crystal fibers," Opt. Express **27**(21), 30798–30809 (2019).
18. J. C. Travers, T. F. Grigorova, C. Brahms, and F. Belli, "High-energy pulse self-compression and ultraviolet generation through soliton dynamics in hollow capillary fibres," Nat. Photonics **13**(8), 547–554 (2019).
19. C. Brahms, T. Grigorova, F. Belli, and J. C. Travers, "High-energy ultraviolet dispersive-wave emission in compact hollow capillary systems," Opt. Lett. **44**(12), 2990–2993 (2019).
20. C. Brahms, F. Belli, and J. C. Travers, "Infrared attosecond field transients and UV to IR few-femtosecond pulses generated by high-energy soliton self-compression," Phys. Rev. Res. **2**(4), 043037 (2020).

Optics EXPRESS

21. A. Crego, E. Jarque, and J. San Roman, "Influence of the spatial confinement on the self-focusing of ultrashort pulses in hollow-core fibers," Sci. Rep. **9**(1), 9546 (2019).
22. E. Conejero Jarque, J. San Roman, F. Silva, R. Romero, W. Holgado, M. Gonzalez-Galicia, I. J. Sola, and H. Crespo, "Universal route to optimal few- to single-cycle pulse generation in hollow-core fiber compressors," Sci. Rep. **8**(1), 2256 (2018).
23. A. Forbes, "Structured light from lasers," Laser Photonics Rev. **13**(11), 1900140 (2019).
24. M. Soljačić, S. Sears, and M. Segev, "Self-trapping of "Necklace" beams in self-focusing Kerr media," Phys. Rev. Lett. **81**(22), 4851–4854 (1998).
25. T. D. Grow, A. A. Ishaaya, L. T. Vuong, and A. L. Gaeta, "Collapse and stability of necklace beams in Kerr media," Phys. Rev. Lett. **99**(13), 133902 (2007).
26. C. Rotschild, M. Segev, Z. Xu, Y. V. Kartashov, L. Torner, and O. Cohen, "Two-dimensional multipole solitons in nonlocal nonlinear media," Opt. Lett. **31**(22), 3312–3314 (2006).
27. S. Z. Silahli, W. Walasik, and N. M. Litchinitser, "Necklace beam generation in nonlinear colloidal engineered media," Opt. Lett. **40**(24), 5714–5717 (2015).
28. W. Walasik, S. Z. Silahli, and N. M. Litchinitser, "Dynamics of necklace beams in nonlinear colloidal suspensions," Sci. Rep. **7**(1), 11709 (2017).
29. L. Stoyanov, N. Dimitrov, I. Stefanov, D. N. Neshev, and A. Dreischuh, "Optical waveguiding by necklace and azimuthon beams in nonlinear media," J. Opt. Soc. Am. B **34**(4), 801–807 (2017).
30. Z. Shi, H. Li, and X. Zhu, "Necklacelike solitons formed by manipulating vortex beams in a synthetic structure," J. Opt. Soc. Am. B **36**(8), 2007–2012 (2019).
31. N. B. Aleksić, A. I. Strinić, M. M. Petroski, and M. S. Petrović, "Necklace beams in media with cubic-quintic nonlinearity," Opt. Quantum Electron. **52**(2), 73 (2020).
32. G. Fibich and D. Shpigelman, "Positive and necklace solitary waves on bounded domains," Phys. D **315**, 13–32 (2016).
33. E. A. J. Marcatili and R. A. Schmeltzer, "Hollow metallic and dielectric wave-guides for long distance optical transmission and lasers," Bell Syst. Tech. J. **43**(4), 1783–1809 (1964).
34. B. A. López-Zubieta, E. C. Jarque, I. J. Sola, and J. S. Roman, "Theoretical analysis of single-cycle self-compression of near infrared pulses using high-spatial modes in capillary fibers," Opt. Express **26**(5), 6345–6350 (2018).
35. B. A. López-Zubieta, E. C. Jarque, I. J. Sola, and J. S. Roman, "Spatiotemporal-dressed optical solitons in hollow-core capillaries," OSA Continuum **1**(3), 930–938 (2018).
36. A. M. Perelomov, V. S. Popov, and M. V. Terentev, "Ionization of atoms in an alternating electric field," Sov. Phys. JETP **23**, 924–934 (1966).
37. G. Fibich and A. L. Gaeta, "Critical power for self-focusing in bulk media and in hollow waveguides," Opt. Lett. **25**(5), 335–337 (2000).
38. G. P. Agrawal, *Nonlinear Fiber Optics*, 5th ed (Academic Press, 2013).